Alloys

DOI: 10.1002/anie.200902934

Ferromagnetic Mesostructured Alloys: Design of Ordered Mesostructured Alloys with Multicomponent Metals from Lyotropic Liquid Crystals**

Yusuke Yamauchi, Masaki Komatsu, Minekazu Fuziwara, Yoshihiro Nemoto, Keisuke Sato, Tokihiko Yokoshima, Hiroaki Sukegawa, Kouichiro Inomata, and Kazuyuki Kuroda**

Mesoporous materials[1,2] have attracted worldwide interest because of their outstanding structural characteristics, such as high surface area, narrow pore size distribution, and well-ordered arrangement of mesopores, which are suitable for a wide variety of applications.[3] Significant advances in synthetic approaches have made it possible to synthesize mesoporous materials with various components, such as non-siliceous metal oxides,[4] organosilicas,[5] carbon meterials,[6] and even polymers.[7]

The synthesis of mesoporous materials with magnetic properties has been subject to extensive research.[8] In the presence of an external magnetic field, magnetic mesoporous materials are attracted to the magnet. This magnetic motor effect is indeed attractive for the development of separation technology. Traditionally, magnetic nanoparticles were loaded after the synthesis of mesoporous materials.[9] However, blocking of the mesopores was observed, which prevented effective incorporation of guest species into the mesopores. Several strategies have been reported to overcome this problem. A simple block-copolymer-based "one-pot" self-assembly approach was developed to incorporate magnetic γ-iron oxide nanoparticles in the mesopore walls.[10] However, the amount of the embedded nanoparticles in the framework is limited, which is a serious problem for higher magnetizations. Microspheres consisting of a magnetic nanoparticle core and mesoporous silica shell have attracted particular attention.[11] These characteristics endow them with significant application potential in various fields, such as bioseparation, enzyme immobilization, and diagnostic analysis. Another route is hard-templating, which involves the deposition of metal oxides within original templates, such as mesoporous silica or carbon, and the subsequent removal of the templates.[12–19] This nanocasting approach is widely applicable to the preparation of metal oxides that are difficult to synthesize by conventional pathways. So far, various kinds of magnetic metal oxides, such as CoO,[12] Co_3O_4,[13] Mn_3O_4,[14] NiO,[15] α-Fe_2O_3, γ-Fe_2O_3, Fe_3O_4,[16] and Gd_2O_3,[17] have been prepared. Although these mesoporous metal oxides have magnetic properties, the saturation magnetization has a lower value than that of pure ferromagnetic metals, such as Fe, Co, and Ni. The saturation magnetization of mesoporous materials depends on the compositions and amounts of magnetic phases. Higher magnetization and greater control are much in demand for current separation technology. Furthermore, if we can proportionally change the saturation magnetization just by changing the framework compositions, we can selectively collect particular ferromagnetic mesoporous materials by changing the external magnetic field.

Fe group elements (Ni, Co, and Fe) and Gd are the only ferromagnetic metallic elements at ambient conditions. From a Slater–Pauling curve, Fe has the highest magnetic moment (fcc Ni: 0.6 μ_B/atom, fcc Co: 1.7 μ_B/atom, bcc Fe: 2.2 μ_B/atom).[18] With such multicomponent alloying, more precise control of the magnetization over a wide range and higher

[*] Prof. Dr. Y. Yamauchi, Dr. Y. Nemoto, Dr. K. Sato
World Premier International (WPI) Research Center for Materials Nanoarchitectonics (MANA)
National Institute for Materials Science (NIMS)
Namiki 1-1, Tsukuba, Ibaraki 305-0044 (Japan)
Fax: (+81) 29-860-4706
E-mail: yamauchi.yusuke@nims.go.jp
Homepage: http://www.nims.go.jp/mana/members/independent_scientist/y_yamauchi/index.html

Prof. Dr. Y. Yamauchi, M. Komatsu, Dr. T. Yokoshima, Prof. Dr. K. Kuroda
Department of Applied Chemistry and Major in Nanoscience and Nanoengineering
Faculty of Science & Engineering, Waseda University
Ohkubo 3-4-1, Shinjuku, Tokyo 169-8555 (Japan)
E-mail: kuroda@waseda.jp

Prof. Dr. Y. Yamauchi
PRESTO Science and Technology Agency (JST)
Honcho 4-1-8, Kawaguchi-shi, Saitama 332-0012 (Japan)

Prof. Dr. Y. Yamauchi, M. Fuziwara, Prof. Dr. K. Kuroda
Kagami Memorial Research Institute for Materials Science and Technology
Waseda University
Nishi-waseda 2-8-26, Shinjuku, Tokyo 169-0051 (Japan)

Dr. T. Yokoshima
Nanoelectronics Research Institute
Advanced Industrial Science and Technology (AIST)
1-1-1 Higashi, Tsukuba, Ibaraki 305-8561 (Japan)

Dr. H. Sukegawa, Dr. K. Inomata
Spintronics Group, Magnetic Materials Center
National Institute for Materials Science (NIMS)
1-2-1 Sengen, Tsukuba, Ibaraki 305-0047 (Japan)

[**] We greatly appreciate the reviewers' helpful comments. This study was supported by the Global COE Program "Practical Chemical Wisdom" from the Japanese Ministry of Education, Culture, Sports, Science, and Technology (MEXT). This work was also supported in part by the A3 Foresight Program "Synthesis and Structural Resolution of Novel Mesoporous Materials" from the Japan Society for the Promotion of Science (JSPS).

Supporting information for this article is available on the WWW under http://dx.doi.org/10.1002/anie.200902934.

magnetization are anticipated.[18] Herein, we demonstrate the synthesis of highly ordered multicomponent mesostructured alloys with controllable compositions. By changing the metal compositional ratios, the saturation magnetization could be controlled. This approach is more convenient than hard-templating because the surfactants can be removed by simple extraction using general organic solvents, such as ethanol.[19] Furthermore, by tuning the extraction process, we can leave a small amount of surfactants covering the metal surfaces to avoid oxidation, and those materials can be denoted as mesostructured metals and alloys. Therefore, this method is applicable for a wide range of metals, including base metals, such as Ni, Co, and Fe. Mesostructured NiCo alloys have been prepared and demonstrated to have ferromagnetic properties.[20,21] However, the ordering of mesostructures decreased with the increase of Co content, which is directly correlated with the increase of the magnetizations.[20] Therefore, high-magnetization ordered mesostructured alloys are very valuable. Our electroless deposition of Ni, Co, and Fe species from lyotropic liquid crystals (LLCs) of a non-ionic surfactant can lead to highly ordered mesostructured alloys, even though it is generally more difficult to deposit multicomponent alloys homogeneously because of the potential existence of complicated phases.

The relationship between the LLC compositions and the compositions of the final products is shown in Figure 1. The final products tended to have relatively richer Co content than the starting compositions of the LLCs (Figure 1 a), showing the preferential deposition of Co in the LLCs. It is well known that, in the conventional NiCo electroless deposition system, Co is preferentially deposited owing to anomalous co-deposition, even though Co has a lower standard electrode potential than Ni.[22] This phenomenon is explained by the kinetic effect: that is, the Co ion decreases the deposition rate of Ni, but the deposition rate of the Co is unchanged.[23] The deposition of Fe in the LLC is in accordance with the normal deposition behavior considering the standard electrode potentials of Ni ($E_0 = -0.25$ V) and Fe ($E_0 = -0.44$ V).[22a] There were no significant changes in the boron component for any of the products (Figure 1 b). Consequently, the compositions of the products can be tuned by changing the metal compositions in LLCs of highly concentrated surfactants.

From the low-angle XRD patterns of the products after extraction at low diffraction angles, all of the products exhibit a broad peak at around 1.7° ($d \approx 7$ nm), indicating the formation of ordered mesostructures despite the difference of the starting LLC compositions (Figure S1 in the Supporting Information). There is no significant loss in intensity by alloying, suggesting that all the products have similar ordered mesostructures to those of mesoporous Ni.

Spherical particles with a relatively uniform size of about 200 nm were observed for all the products (Figure 2 a,b; all SEM images are shown in Figure S2 in the Supporting Information). The mesostructures were directly observed by transmission electron microscopy (TEM), as is displayed in Figure 2 c (all TEM images are shown in Figure S3 in the Supporting Information). Stripes with a repeated distance of around 8 nm and honeycomb arrangements of mesopores

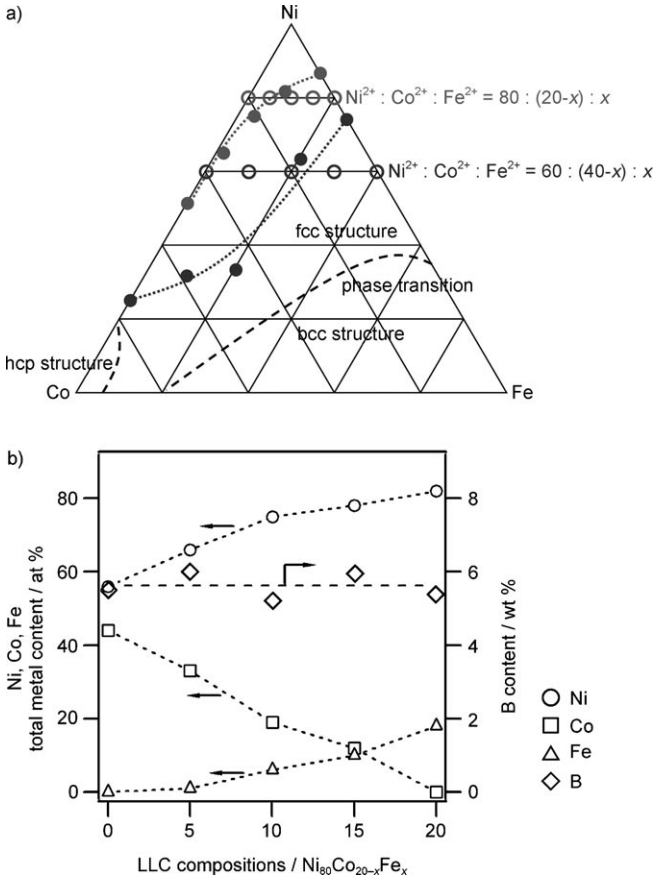

Figure 1. a) Relationship between the compositions of the final products and the LLC compositions before metal deposition. The product compositions were analyzed by ICP analysis. ○: LLC compositions, ●: product compositions. b) Variation of product compositions (Ni, Co, Fe, and B) prepared from the LLC compositions ($Ni^{2+}/Co^{2+}/Fe^{2+} = 80{:}20{-}x{:}x$). The product compositions were analyzed by ICP analysis.

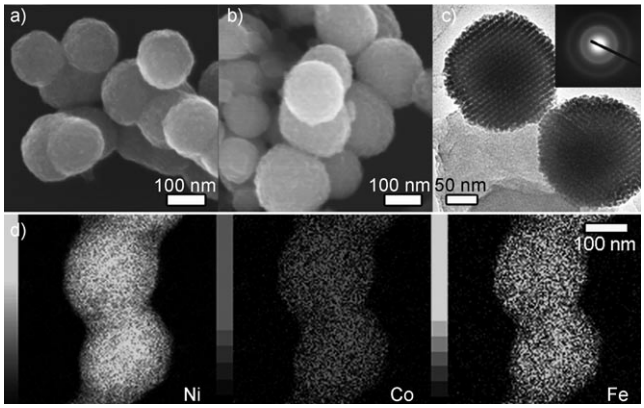

Figure 2. a) SEM images of mesostructured alloys prepared from different LLC compositions. a) $Ni_{77}Co_9Fe_8B_6$ alloy prepared from the LLC composition $Ni^{2+}/Co^{2+}/Fe^{2+} = 80{:}5{:}15$. b) $Ni_{78}Fe_{16}B_6$ alloy prepared from the LLC composition $Ni^{2+}/Fe^{2+} = 80{:}20$. c) TEM image and the corresponding ED patterns (inset) of $Ni_{62}Co_{30}Fe_2B_6$ alloy prepared from LLC composition $Ni^{2+}/Co^{2+}/Fe^{2+} = 80{:}15{:}5$. d) EDS mappings of $Ni_{71}Co_{17}Fe_6B_6$ alloy prepared from the LLC composition $Ni^{2+}/Co^{2+}/Fe^{2+} = 80{:}10{:}10$.

were clearly observed over the entire area. The distance between the mesopores, calculated from the tentatively assigned (10) peak ($d = 7.0$ nm), is 8.1 nm ($7.0 \times 2/\sqrt{3}$), which is in agreement with the value obtained from these TEM images. The BET specific surface areas calculated from N_2 adsorption–desorption isotherms were around 80–90 $m^2 g^{-1}$ (a representative isotherm is shown in Figure S4 in the Supporting Information). The pore size distributions, as determined by BJH (Barrett–Joyner–Halenda) analysis of the adsorption curves, were in the range 2–4 nm.

Figure 2d shows the energy dispersive X-ray spectroscopy (EDS) mappings of the product ($Ni_{71}Co_{17}Fe_6B_6$) prepared from the starting LLC of $Ni^{2+}/Co^{2+}/Fe^{2+} = 80:10:10$. Each metal is distributed homogeneously over the entire spherical particle without separation of the nanoscale phases (the high-resolution nanoscale EDS mapping is shown in Figure S5 in the Supporting Information). The product composition calculated from the EDS was in good agreement with the ICP (inductively coupled plasma) results (Figure 1). A notable signal assigned to oxygen did not appear. Although the sensitivity of light elements (oxygen) in EDS analysis is low, it is strongly suggested that metals are in general not oxidized. The selected-area electron diffraction (ED) pattern (Figure 2c) also indicates no formation of Ni, Co, and Fe oxide compounds.

To investigate the crystallinity of the pore walls, a high-angle XRD measurement was performed (Figure S1 in the Supporting Information). Broad diffraction peaks for all the samples were observed at 35–55°, which corresponded to the (111) plane of the fcc structure. Generally, metal deposition processes using boron-containing reducing agents result in the incorporation of the B component into the alloys. As the B content is increased (typically higher than 3 wt%), the deposits tend to have a poorly crystalline state that results in a broad diffraction peak in the high-angle range.[24] The peak intensities of ternary alloys composed of Ni, Co, and Fe were lower than those of binary alloys (Figure S1) as a result of a decrease of the crystalline size in the pore wall owing to the formation of more complicated phases such as Ni-based fcc phases with relatively richer Co or Fe components as well as metal boride amorphous phases.[25] The grain sizes of the products were roughly estimated by a Scherrer equation to be smaller than 2 nm, indicating that the pore walls are composed of minute crystalline sizes or that they are in an amorphous-like state.[26]

It is noteworthy that, for the product ($Ni_{78}Fe_{16}B_6$) from the starting LLC composition of $Ni^{2+}/Co^{2+}/Fe^{2+} = 80:0:20$, the as-deposited product shows other noticeable peaks at $2\theta = 11°$, 22°, 33°, and 60°, which are assignable to be green rust I, Fe-based layered double hydroxide. The Fe ions in the solution are in equilibrium between Fe^{2+} and Fe^{3+}. In addition, the heating process needed for production of the homogenous LLCs could be responsible for the formation of Fe^{3+}. When the reducing agent dimethylamine borane (DMAB) was added to the LLC, the pH rose above 7. Under those conditions, the Fe species tend to form green rust I ($Fe^{II}_x Fe^{III}_y (O,OH,Cl)_z$). Although the green rust I is unstable in ambient air owing to further oxidation to $Fe^{III}OOH$,[27] the presence of Ni ions leads to the formation of Ni-substituted green rust I ($Ni^{II}_x Fe^{III}_y (O,OH,Cl)_z$), which is more stable in ambient air.[28] Thus, when the Fe species are highly concentrated, the formation of green rust I is inevitable. However, green rust I can be easily collected by utilizing the magnetic properties of the product, because the mesostructured alloys are magnetic, whereas green rust I is not. The separated product shows no peaks assignable to green rust I, meaning that the separation technique using a magnet is highly useful to obtain only pure mesoporous magnetic alloys (Figure S6 in the Supporting Information). The local crystalline structures were determined from the selected ED patterns in Figure S7. The ED patterns of the ordered mesostructured particle showed ring patterns. In the high-resolution TEM image, the lattice fringes assigned to a fcc structure were randomly oriented in the mesostructured alloy (Figure S8). The walls are composed of very minute crystalline sizes, as also supported by high-angle XRD patterns (Figure S1). Although the crystallinity of the particles can be improved by annealing under an inert atmosphere, the ordered mesostructures collapse. The ordered mesostructure is stable up to 150 °C under N_2 atmosphere. In contrast, the ED patterns of the needle-like parts (of the by-products, green rust I) showed rings with hexagonal spots. These d spacings in these patterns coincided well with those of the high-angle XRD patterns of green rust I (Figure S1).

Magnetic NiCoFeB alloys with highly ordered mesostructures should be useful for future magnet-based science and technology. Figure 3a shows the change in the saturation magnetization (M_s) of the mesoporous alloys prepared under various LLC compositions ($Ni^{2+}/Co^{2+}/Fe^{2+} = 80:20–x:x$). In the present system, the pore walls in the products are composed of very minute crystalline sizes or an amorphous-like state, as observed in the wide-angle XRD patterns and selected area ED patterns. It is generally known that very small ferromagnetic grains show superparamagnetic behavior; that is, each grain does not show a ferromagnetic state because of the thermal fluctuation of the magnetic moment at room temperature. No hysteresis was observed in the magnetization curve (Figure 3; the coercive forces (H_c) and residual magnetization (M_r) were almost zero), which is typical of superparamagnetic behavior.

In general, M_s values gradually increase with an increase in the grain size. The grain size of ternary alloys (consisting of Ni, Co, and Fe) was smaller than that of binary alloys (Figure S1). However, in this study, the M_s value increased proportionally with the Fe content independently of the grain size. In the present case, therefore, the metal composition has a greater effect than the grain size. This relationship between the metal compositions and M_s value is similar to that of annealed NiCoFe bulk alloys.[18c] In addition, the Slater–Pauling curve shows an increase in the magnetic moment proportionally with the number of electrons; that is, the magnetic moment of Fe is higher than that of Co and Ni. Consequently, the M_s values in the mesoporous alloys (Figure 3a) changed.

Highly ordered mesostructured alloys showed magnetization up to 56 emu g^{-1}, whereas mesostructured $Ni_{94}B_6$ showed very small magnetization (0.11 emu g^{-1}). This value is the highest M_s value of all magnetic mesostructured

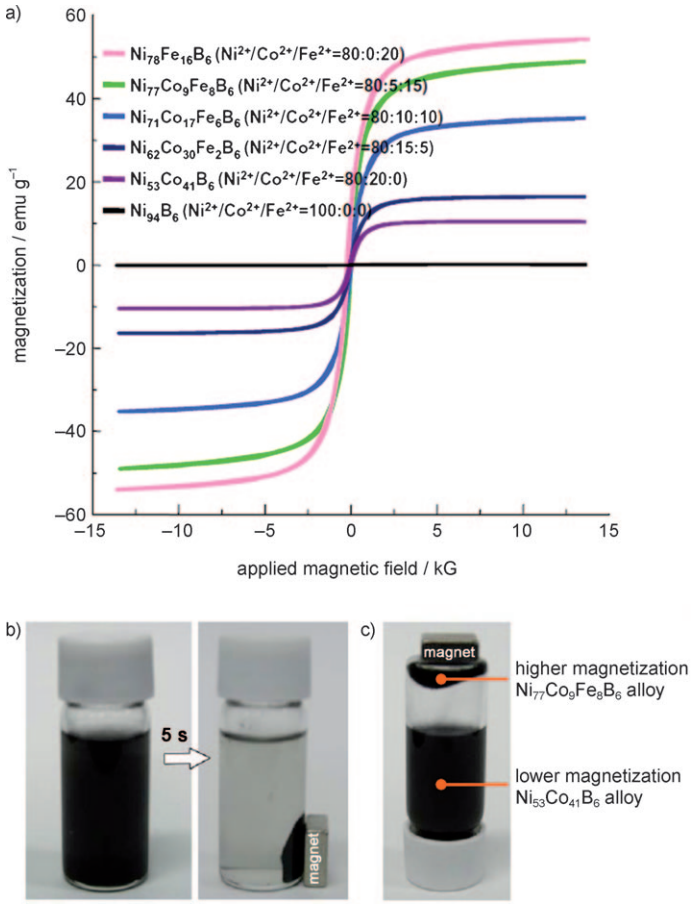

Figure 3. a) Magnetic hysteresis loops of mesostructured alloys prepared from different LLC compositions. The LLC compositions are shown in parentheses. b,c) Investigation of the magnetic response.

materials to date.[9–10,12–17] It is also sufficient for magnetic attraction by a commercial magnet. The dispersed mesostructured alloys moved very quickly toward the applied neodymium magnet (around 1000 Oe), showing excellent magnetic responsivity (Figure 3b). The saturation magnetization of mesostructured alloys can also be controlled by changing the framework compositions. For example, two types of magnetic alloys with different magnetization were mixed in the solutions. By changing the applied magnetic force, we could selectively collect higher magnetization alloy particles, which is an advantage for their future applications (Figure 3c).

To achieve higher saturation magnetization, it is more effective to lower the content of Ni and increase the amount of Co and Fe.[18] Therefore, in preliminary work, further experiments were carried out with an increase in the compositions of Co and Fe in the starting LLC. The products obtained after deposition of the mesoporous alloys were separated with a magnet.

In the LLC system of $Ni^{2+}/Co^{2+}/Fe^{2+} = 60{:}40{-}x{:}x$, the composition of the products was controlled by changing the metal compositions in the LLC (Figure S9 in the Supporting Information). From the XRD pattern (Figure S10), we found that the mesostructural ordering of the products greatly decreased upon further alloying, although there was no significant difference in the crystal structures suggested from the higher-angle XRD patterns. The products were identified by TEM (Figure S11) to have less ordered and disordered mesostructures with irregular morphologies. These results are mainly due to the difference in the catalytic activity of the reducing agent dimethylamine borane (DMAB).[29] The catalytic activity of DMAB for the reduction of Ni is higher than that of Co and Fe. Therefore, with a higher composition of Ni in LLC, an autocatalytic reaction predominantly proceeds to form spherical particulate alloys with the retention of ordered mesophases of the LLC by the isotropic reduction of metal species.[21] However, as the composition of Ni in LLC decreases, the rate of the autocatalytic reaction of Ni is relatively decelerated, and the self-decomposition reaction of DMAB occurs to some extent. As a consequence, the mesostructures of the LLC could not be retained, and disordered mesostructures with irregular morphologies were observed as a result of more random reduction.[21] The presence of Co ions during the Ni deposition leads to the lowering of the Ni reduction rate; consequently, the compositions of the products deposited from LLC including relatively lower Ni and higher Co ions had a very small Ni content relative to the starting LLC compositions (Figure S9).

To conclude, we synthesized mesostructured multicomponent (Ni, Co, and Fe) magnetic alloy particles using a non-ionic surfactant as a soft template. By simply changing the starting LLC compositions, uniform-size alloy particles with tunable compositions could be obtained. This understanding of the synthesis of multicomponent mesostructured alloys should greatly contribute to the future fabrication of mesoporous metals with desired functions. Although many mesoporous metals, such as Pt, Sn, Cu, and Ni, have been synthesized from LLCs,[30–40] their major applications have been limited to electrodes and catalysts. New functions that are not found in a single metal system can be realized by alloying. The synthesis of mesoporous alloys with desired elements and compositional ratios should give rise to a new class of mesoporous metals. This study should open the door to new magnetic applications.

Experimental Section

Materials: A non-ionic surfactant ($C_{16}EO_{10}$, Brij 56, Aldrich) was used to form lyotropic liquid crystals. Nickel(II) chloride ($NiCl_2$ >98%, Aldrich), cobalt(II) chloride ($CoCl_2$ >95%, Kanto Kagaku Co.), and iron(II) chloride tetrahydrate ($FeCl_2{\cdot}4H_2O$ >98%, Kanto Kagaku Co.) were used as metal sources. Sodium borohydride ($NaBH_4$ >98%, Kanto Kagaku Co.) and dimethylamine borane (DMAB) ($(CH_3)_2HNBH_3$ >97%, Fluka Co.) were used as reducing agents. Ethanol (H_2O content <0.005%, Junsei Chemical Co.) was used to remove excess reducing agent, undeposited metal ions, and surfactants.

Synthesis of mesostructured alloys: First, a precursor was prepared by dissolving metal species of various compositions (0.01 mol) in deionized water (3.3 g) and adding non-ionic surfactant Brij56 (4.0 g) in a closed container. The water content in the LLC is very important for the formation of the ordered mesophases.[41] To avoid evaporation of the water, we used a closed container. The mixtures were heated to 60 °C, which is above the melting point of Brij56, until the mixture became homogeneous. Cooling the mixtures formed a homogeneous LLC phase with a 2D hexagonal structure,

which was characterized by polarization optical microscopic observation and low-angle XRD measurements. In this LLC mesophase, dissolved metal ions are coordinated by water molecules to form metal aqua complexes. Hydrogen bonds between ethylene oxide groups of surfactants and coordinated water molecules are formed, thus stabilizing the metal aqua complexes in the LLC.[41] The metal species in the presence of LLC was reduced by the addition of combined reducing agents (0.4 g of DMAB and 0.001 g of $NaBH_4$). At the initial stages of metal deposition, electrons spontaneously are generated by self-decomposition of $NaBH_4$. Very small amounts of metal nuclei were deposited over the entire area of the LLC. Then, the DMAB molecules are adsorbed onto Ni atoms (not Co and Fe atoms) of the deposited nuclei and subsequently provide electrons, because the catalytic activity of DMAB on Ni surface is higher than those of DMAB on Co and Fe surface. Thus, the metal deposition (i.e., autocatalytic reaction) from the nuclei proceeds to coat the rodlike self-assemblies in the LLC.[21] The deposits were rinsed with ethanol three times to remove excess undeposited metal species and reducing agents. After the metal ions were reduced, the deposited alloys do not strongly interact with surfactant chains or physically contact the surfactant chains. Therefore, the surfactant can be removed by washing with ethanol. After rinsing in dehydrated ethanol, almost all surfactants were removed, and only 2–3 wt % of C remained in the final products.

Characterization: Powder XRD patterns at low diffraction angles were measured using a Mac Science M03XHF22 diffractometer with Mn-filtered $Fe_{K\alpha}$ radiation (40 kV, 20 mA) at a scanning rate of $0.5° min^{-1}$. High diffraction angle XRD patterns were measured using a Mac Science MXP3 diffractometer with $Cu_{K\alpha}$ radiation (40 kV, 30 mA) equipped with monochromator at a scanning rate of $1° min^{-1}$. FE-SEM images were obtained by a JEOL JSM-6500F scanning electron microscope operated at an accelerating voltage of 15 kV. EDS mapping analysis was conducted with a JEM-2100F scanning transmission electron microscope operated at an accelerating voltage of 200 kV. TEM images were obtained by a JEOL JEM-2010 transmission electron microscope operated at an accelerating voltage of 200 kV. The samples for electron microscopy were prepared by dispersing the powder products in ethanol and mounting them onto a Si substrate for FE-SEM and on a microgrid for TEM. The remaining surfactant was analyzed by CHN analysis using a Perkin–Elmer PE2400II. The compositions of the products were determined by ICP using the Japan Jarrell-Ash IRIS-AP.

Received: June 1, 2009
Revised: July 18, 2009
Published online: September 10, 2009

Keywords: alloys · liquid crystals · magnetic properties · mesoporous materials

[1] T. Yanagisawa, T. Shimizu, K. Kuroda, C. Kato, *Bull. Chem. Soc. Jpn.* **1990**, *63*, 988.
[2] C. T. Kresge, M. E. Leonowicz, W. J. Roth, J. C. Vartuli, J. S. Beck, *Nature* **1992**, *359*, 710.
[3] A. Vinu, T. Mori, K. Ariga, *Sci. Technol. Adv. Mater.* **2006**, *7*, 753.
[4] a) Q. Huo, D. I. Margolese, U. Ciesla, P. Feng, T. E. Gler, P. Sieger, R. Leon, P. M. Petroff, F. Schuth, G. D. Stucky, *Nature* **1994**, *368*, 317; b) D. M. Antonelli, J. Y. Ying, *Angew. Chem.* **1995**, *107*, 2202; *Angew. Chem. Int. Ed. Engl.* **1995**, *34*, 2014.
[5] a) S. Inagaki, S. Guan, T. Ohsuna, O. Terasaki, *Nature* **2002**, *416*, 304; b) Y. Wan, D. Zhang, Y. Zhai, C. Feng, J. Chen, H. Li, *Chem. Asian J.* **2007**, *2*, 875.
[6] a) R. Ryoo, S. H. Joo, S. Jun, *J. Phys. Chem. B* **1999**, *103*, 7743; b) C. H. Ko, R. Ryoo, *Chem. Commun.* **1996**, 2467.
[7] Y. Meng, D. Gu, F. Zhang, Y. Shi, H. Yang, Z. Li, C. Yu, B. Tu, D. Zhao, *Angew. Chem.* **2005**, *117*, 7215; *Angew. Chem. Int. Ed.* **2005**, *44*, 7053.
[8] a) S. Giri, B. G. Trewyn, M. P. Stellmaker, V. S. Y. Lin, *Angew. Chem.* **2005**, *117*, 5166; *Angew. Chem. Int. Ed.* **2005**, *44*, 5038; b) J. W. Long, M. S. Logan, C. P. Rhodes, E. E. Carpenter, R. M. Stroud, D. R. Rolison, *J. Am. Chem. Soc.* **2004**, *126*, 16879.
[9] a) M. Fröba, R. Köhn, G. Bouffaud, O. Richard, G. van Tendeloo, *Chem. Mater.* **1999**, *11*, 2858; b) L. Zhang, G. C. Papaefthymiou, J. Y. Ying, *J. Phys. Chem. B* **2001**, *105*, 7414.
[10] C. Garcia, Y. Zhang, F. DiSalvo, U. Wiesner, *Angew. Chem.* **2003**, *115*, 1564; *Angew. Chem. Int. Ed.* **2003**, *42*, 1526.
[11] a) Y. Deng, D. Qi, C. Deng, X. Zhang, D. Zhao, *J. Am. Chem. Soc.* **2008**, *130*, 28; b) T. Sen, A. Sebastianelli, I. J. Bruce, *J. Am. Chem. Soc.* **2006**, *128*, 7130.
[12] H. Tüysüz, Y. Liu, C. Weidenthaler, F. Schüth, *J. Am. Chem. Soc.* **2008**, *130*, 14108.
[13] a) B. Z. Tian, X. Lui, L. Solovyov, Z. Liu, H. Yang, Z. Zhang, S. Xie, F. Zhang, B. Tu, C. Yu, O. Terasaki, D. Zhao, *J. Am. Chem. Soc.* **2004**, *126*, 865; b) Y. Wang, C. M. Yang, W. Schmidt, B. Spliethoff, E. Bill, F. Schüth, *Adv. Mater.* **2005**, *17*, 53; c) H. Tüysüz, C. W. Lehmann, H. Bongard, R. Schmidt, B. Tesche, F. Schüth, *J. Am. Chem. Soc.* **2008**, *130*, 11510.
[14] F. Jiao, A. Harrison, A. H. Hill, P. G. Bruce, *Adv. Mater.* **2007**, *19*, 4063.
[15] F. Jiao, A. H. Hill, A. Harrison, A. Berko, A. V. Chadwick, P. G. Bruce, *J. Am. Chem. Soc.* **2008**, *130*, 5262.
[16] a) F. Jiao, A. Harrison, J. C. Jumas, A. V. Chadwick, W. Kockelmann, P. G. Bruce, *J. Am. Chem. Soc.* **2006**, *128*, 5468; b) F. Jiao, J. C. Jumas, M. Womes, A. V. Chadwick, A. Harrison, P. G. Bruce, *J. Am. Chem. Soc.* **2006**, *128*, 12905.
[17] M. Yada, H. Kitamura, A. Ichinose, M. Machida, T. Kijima, *Angew. Chem.* **1999**, *111*, 3716; *Angew. Chem. Int. Ed.* **1999**, *38*, 3506.
[18] a) T. Osaka, M. Takai, K. Hayashi, K. Ohashi, M. Saito, K. Yamada, *Nature* **1998**, *392*, 796; b) T. Osaka, T. Yokoshima, T. Nakanishi, *IEEE Trans. Magn.* **2001**, *37*, 1761; c) *Iron-Cobalt-Nickel Alloys in Ferromagnetism* (Ed.: R. M. Bozorth), Wiley-VCH, Weinheim, **1993**, pp. 160–169.
[19] a) G. S. Attard, P. N. Bartlett, N. R. B. Coleman, J. M. Elliott, J. R. Owen, J. H. Wang, *Science* **1997**, *278*, 838; b) Y. Yamauchi, K. Kuroda, *Chem. Asian J.* **2008**, *3*, 664.
[20] Y. Yamauchi, T. Yokoshima, T. Momma, T. Osaka, K. Kuroda, *J. Mater. Chem.* **2004**, *14*, 2935.
[21] a) Y. Yamauchi, T. Yokoshima, H. Mukaibo, M. Tezuka, T. Shigeno, T. Momma, T. Osaka, K. Kuroda, *Chem. Lett.* **2004**, *33*, 542; b) Y. Yamauchi, T. Momma, T. Yokoshima, K. Kuroda, T. Osaka, *J. Mater. Chem.* **2005**, *15*, 1987.
[22] a) G. Milazzo, S. Caroli, Tables of Standard Electrode Potentials, Wiley, New York, **1978**, pp. 336–349; b) N. Fukumuro, M. Tikazawa, T. Watanabe, *J. Surf. Finish. Soc. Jpn.* **1999**, *50*, 441.
[23] C. Fan, D. L. Piron, *Electrochim. Acta* **1996**, *41*, 1713.
[24] T. Saito, E. Sato, M. Matsuoka, C. Iwakura, *J. Appl. Electrochem.* **1998**, *28*, 559.
[25] S. Chikazumi, K. Ohta, K. Adachi, N. Tsuya, Y. Ishikawa, *Handbook of Magnetic Substance*, Asakura Press, Tokyo, **1975**, p. 331.
[26] The Scherrer equation is basically applicable when crystalline sizes are larger than 50 nm. However, it has recently been applied to spherical nanoparticles with sizes of a few nanometers. It has been reported that the values calculated by the Scherrer equation are almost identical to those observed using TEM. Therefore, herein, we used it to roughly calculate the grain size in the frameworks.
[27] R. M. Cornell, U. Schwertmann, *The Iron Oxides*, 2nd ed., Wiley-VCH, New York, **2003**.

[28] P. Refait, H. Drissi, Y. Marie, J. M. R. Genin, *Hyperfine Interact.* **1994**, *90*, 389.
[29] I. Ohno, O. Wakabayashi, S. Haruyama, *J. Electrochem. Soc.* **1985**, *132*, 2323.
[30] P. N. Bartlett, P. N. Birkin, M. A. Ghanem, P. de Groot, M. Sawicki, *J. Electrochem. Soc.* **2001**, *148*, C119-C123.
[31] H. M. Luo, L. Sun, Y. F. Lu, Y. S. Yan, *Langmuir* **2004**, *20*, 10218 – 10222.
[32] a) P. A. Nelson, J. M. Elliott, G. S. Attard, J. R. Owen, *Chem. Mater.* **2002**, *14*, 524; b) V. Ganesh, V. Lakshminarayanan, *Electrochim. Acta* **2004**, *49*, 3561 – 3572; c) R. Campbell, M. G. Bakker, *J. Porous Mater.* **2004**, *11*, 63 – 69; d) D. D. Zhao, W. J. Zhou, H. L. Li, *Chem. Mater.* **2007**, *19*, 3882 – 3891.
[33] H. M. Luo, J. F. Zhang, Y. S. Yan, *Chem. Mater.* **2003**, *15*, 3769 – 3773.
[34] F. Bender, R. K. Mankelow, D. B. Hibbert, J. J. Gooding, *Electroanalysis* **2006**, *18*, 1558 – 1563.
[35] a) P. N. Bartlett, B. Gollas, S. Guerin, J. Marwan, *Phys. Chem. Chem. Phys.* **2002**, *4*, 3835 – 3842; b) T. Imokawa, K. J. Williams, G. Denuault, *Anal. Chem.* **2006**, *78*, 265 – 271.
[36] P. N. Bartlett, J. Marwan, *Microporous Mesoporous Mater.* **2003**, *62*, 73 – 79.
[37] P. N. Bartlett, J. Marwan, *Chem. Mater.* **2003**, *15*, 2962 – 2968.
[38] P. A. Nelson, J. R. Owen, *J. Electrochem. Soc.* **2003**, *150*, A1313 – A1317.
[39] A. H. Whitehead, J. M. Elliott, J. R. Owen, G. S. Attard, *Chem. Commun.* **1999**, 331 – 332.
[40] a) J. M. Elliott, P. R. Birkin, P. N. Bartlett, G. S. Attard, *Langmuir* **1999**, *15*, 7411 – 7415; b) S. A. G. Evans, J. M. Elliott, L. M. Andrews, P. N. Bartlett, P. J. Doyle, G. Denuault, *Anal. Chem.* **2002**, *74*, 1322 – 1326; c) S. Park, T. D. Chung, H. C. Kim, *Anal. Chem.* **2003**, *75*, 3046 – 3049; d) H. Boo, S. Park, B. Ku, Y. Kim, J. H. Park, H. C. Kim, T. D. Chung, *J. Am. Chem. Soc.* **2004**, *126*, 4524 – 4525; e) J. Jiang, A. Kucernak, *Electrochem. Solid-State Lett.* **2000**, *3*, 559 – 562; f) M. Y. Nie, J. M. Elliott, *J. Mater. Sci. Technol.* **2005**, *21*, 863 – 865; g) A. Saramat, M. Andersson, S. Hant, P. Thormählen, M. Skoglundh, G. S. Attard, A. E. C. Palmqvist, *Eur. Phys. J. D* **2007**, *43*, 209 – 211.
[41] a) Ö. Çelik, Ö. Dag, *Angew. Chem.* **2001**, *113*, 3915 – 3919; *Angew. Chem. Int. Ed.* **2001**, *40*, 3799 – 3803; b) Ö. Dag, O. Samarskaya, C. Tura, A. Günay, Ö. Çelik, *Langmuir* **2003**, *19*, 3671 – 3676; c) Ö. Dag, S. Alayoğlu, İ. Uysal, *J. Chem. Phys. B* **2004**, *108*, 8439 – 8446; d) C. Albayrak, G. Gülten, Ö. Dag, *Langmuir* **2007**, *23*, 855 – 860.

